J Therm Spray Tech (2024) 33:882–894
https://doi.org/10.1007/s11666-024-01719-1

ORIGINAL RESEARCH ARTICLE

Polymer Metallization by Cold Spray Deposition of Polyamide-Copper Composite Coatings

Maniya Aghasibeig[1] · Abdelkader Benhalima[1] · Kintak Raymond Yu[1]

Submitted: 27 October 2023 / in revised form: 18 December 2023 / Accepted: 27 December 2023 / Published online: 6 February 2024

Abstract Cold spray metallization of polymers is a promising surface engineering technique that enables the deposition of metal coatings onto polymer substrates at low process temperatures, resulting in improved surface properties, thus enhanced functionality of the polymeric material. However, deposition of well-adhering metallic coatings without causing surface damage to the polymer substrate is still a challenge. In this work, copper-polyamide composite coatings with different copper concentrations between 30 and 75 vol.% in the starting powders were deposited on polyamide substrates using a low-pressure cold spray system with two nozzle geometries of short and long diverging sections. The spray parameters were first developed for the deposition of polyamide powder (at gas temperature of 260 °C and gas pressures ranging from 0.41 to 1.37 MPa), and then used to spray the composite powder mixtures where the polyamide particles were acting as a binder for copper particles. Inflight and impact particle characteristics (velocity and temperature) of the polyamide powder were simulated to better understand the deposition properties. Considering that the selected conditions were suboptimal for the deposition of copper particles, no surface damage was caused as no penetration of the copper particles into the polymer substrate occurred. The results show that increasing the copper content in the powder mixtures significantly improved the resulting coating uniformity and the retained copper content. In addition, the coating deposited by spraying the powder mixture with a higher copper content of 75 vol.% and using the longer nozzle yielded the highest cohesion strength. To further improve coatings cohesion, two post-spray processing methods of furnace heating and hot pressing were used, and the effect of each process on coatings properties was investigated.

Keywords cold spray · copper · composite coatings · polymer metallization · polyamide

Introduction

Polymer-based composites offer excellent strength and stiffness to weight ratios, high resistance to corrosion, design flexibility, and can be used to produce large and structurally complex parts, lowering assembly costs (Ref 1, 2). They are therefore widely used in a broad range of transportation structural applications such as automobiles, aircrafts, helicopters spacecrafts, boats and energy sector applications such as wind turbines (Ref 1). Due to the increasing demand for lightweighting and fuel efficiency, aerospace and automotive industries are shifting toward greater use of plastics and composite parts (Ref 1-3). Despite the important advantages that polymer-based materials are offering, certain limitations related to their low wear resistance as well as their lack of electrical and thermal conductivity still need to be overcome to extend their use in new and established applications, such as lightning strike protection, electromagnetic shielding and antifouling coatings (Ref 4-6). Surface metallization of polymer-based materials is recognized as an effective technique to overcome these performance limitations.

In recent years, cold spray has been widely investigated for the deposition of conductive coatings on polymers (Ref 5, 7-10). Cold spray is a solid-state deposition process in

✉ Maniya Aghasibeig
Maniya.Aghasibeig@cnrc-nrc.gc.ca

[1] National Research Council Canada, Boucherville, QC, Canada

which the feedstock powder particles, accelerated to high velocities by a supersonic gas jet flowing through a convergent-divergent de Laval nozzle, form a deposit layer upon high kinetic energy impact on the surface of a substrate (Ref 11-13). Due to the low process temperatures of cold spray, the risk of thermal degradation of the polymeric substrates is minimized (Ref 7). The main challenge of using cold spray for the metallization of polymers is low adhesion strength between the metallic particles and the substrate. Although successful deposition of low melting point metal powders such as tin and zinc has been reported, deposition of metallic materials of higher melting temperature and hardness such as copper and aluminum is still challenging due to excessive surface erosion and structural damage of the polymer surface by high velocity impact of hard particles (Ref 4, 14-17). To minimize or prevent surface damage, mild to low process parameters need to be used when spraying on polymers resulting in lower kinetic energy of particles at impact, thus low coating deposition efficiency. In addition, due to the formation of high level of porosity and inter-particle defects at low process conditions the coating exhibits low adhesion and cohesion strength and low electrical conductivity (Ref 16, 18). The potential solution of adding an interlayer between the polymer and the metallic coating has been investigated in several studies. This interlayer acts as a protective layer against surface erosion during the spray process, while it promotes adhesion in between the metal coating and the substrate. From literature, interlayers of co-cured copper particles with substrate, electroplated copper and cold sprayed interlayers of low melting point metals have been reported to improve coating adhesion and buildup (Ref 18-23). Addition of a secondary metallic component of a higher hardness such as aluminum, copper and zinc to a softer metal powder such as tin is another solution that has been proven to improve the deposition process via inducing shot peening effect (Ref 24-27). Using a similar approach, composite coatings of metal-polymer have been deposited via cold spraying of their powder mixtures. In this case, the polymer matrix within the composite coating acts as a binder for the embedded metal particles allowing coating buildup and promoting both coating adhesion and cohesion, while the deposited metallic particles provide the electrical properties (Ref 28, 29).

In this study, cold spray deposition of dense and uniform copper-rich coatings on polyamide−6 (PA6) substrates was investigated. The window of deposition was first identified for the polyamide−6 powder without copper addition. The effect of different process parameters and nozzle geometries on particles velocity and temperature at the impact point, which affect the resulting coating quality, was evaluated. For each nozzle geometry, the optimum spray condition that yielded dense polymer coatings with high surface quality was identified and employed for the deposition of the copper-PA6 composite powders of different copper content. Two approaches of furnace heat treatment and hot pressing were used to improve the cohesion strength of the coatings. The coatings were then characterized in terms of their microstructures and adhesion/cohesion strength.

Materials and Methods

Feedstock Powders Characterization

Commercially available Polyamide−6 (PA6, Goodfellow, USA; d_{10}: 14 µm, d_{50}: 20 µm, d_{90}: 29 µm) and gas atomized copper (Cu, Sandvik, USA; d_{10}: 5 µm, d_{50}: 12 µm, d_{90}: 20 µm) powders were used in this study. Particle size distribution (PSD) of the powders measured with a laser diffraction particle sizing analyzer (Beckman, USA) is shown in Fig. 1. The PSD analysis demonstrates a regular size distribution of PA6 powder suitable for cold spray while Cu powder presents a smaller PSD. SEM micrographs in Fig. 2 show that the copper powder has spherical shape whereas the PA6 powder is composed of mostly irregular shaped particles with rough surface features.

A differential scanning calorimetry (DSC) was used to determine the thermal transition of PA6, glass transition (T_g), melting (T_m) and crystallization (T_c) temperatures. DSC analysis was performed with a DSC Q2000 instrument (TA Instruments, USA) according to the following protocol: samples were heated from − 30 to 280 °C at a heating rate of 10 °C/min, held for 1 min at 280 °C and then cooled to − 30 °C at a cooling rate of 10 °C/min. The heating-cooling cycle was repeated afterward. All the tests were run under 50 mL/min nitrogen flow.

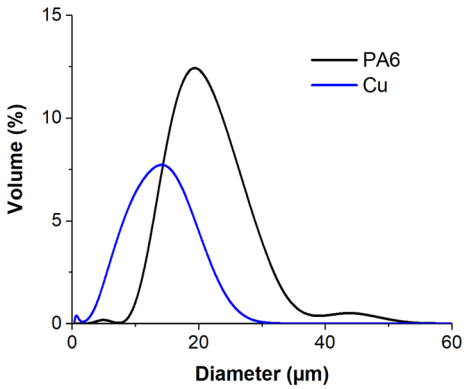

Fig. 1 Particle size distribution of the feedstock powders

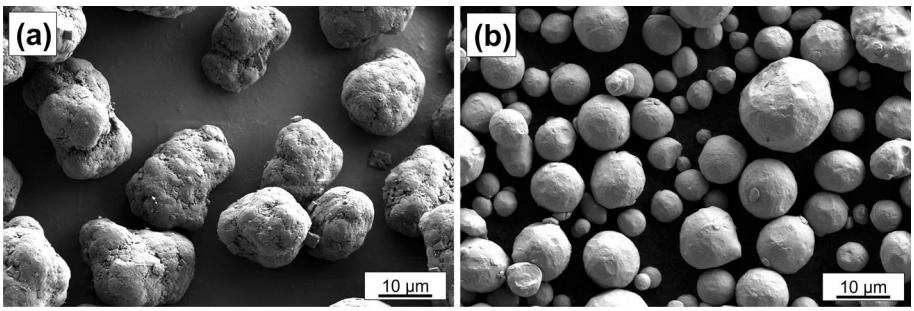

Fig. 2 SEM 3D micrographs of (a) polyamide−6 and (b) copper feedstock powders

Cold Spray Coating Deposition

A Centerline low pressure cold spray system (SST, Centerline, Canada) was employed for the deposition process using nitrogen as the propelling gas. The downstream feeding (powder injection into the diverging section of the nozzle) of the Centerline system makes is suitable for spraying materials with low melting points such as PA6 due to the minimized risk of nozzle clogging. Sprays were performed using two different nozzle geometries that will be referred herein as the short and long nozzles. The difference between the two nozzles was in the length of the diverging section and the outlet diameter. The nozzle divergence length was 230 mm for the long nozzle and 146 mm for the short nozzle. Both nozzles with identical throat diameter, had the same ratio of divergence length to outlet diameter of 23.

The window of deposition was first developed for spraying of the PA6 powder and it was then extended to the spraying of PA6-Cu composite powders. All coatings were deposited at a standoff distance of 10 mm using a step size of 1 mm. Powders were pre-heated to 40 °C in the feeder to promote particle heating in the gas jet and deformation at impact. The feed rate of the PA6 powder was selected at 4 g/min. The effect of cold spray gas temperature, gas pressure and traverse speed (TS) on the deposition properties of the PA6 powder was investigated using the parameters presented in Table 1. For each spray condition, a 10 to 15 mm wide strip was deposited on rectangular PA6 substrates (McMaster-Carr, USA) of dimensions 25.4 × 50.8 × 6.4 mm. Prior to each spray, the surface of the substrate was manually grinded using an 80-grit sand paper to obtain a surface roughness of ∼ 6 µm and the surface was cleaned with ethanol. The optimum spray condition was selected based on the top surface deposition quality (uniformity and smoothness), which was significantly affected by even a small change in the spray parameters.

Three powder mixtures with 30, 50 and 75 vol.% of Cu (77.3, 88.8 and 96 wt.%, respectively) were prepared for the deposition of PA6-Cu composite coatings, using the optimum spray condition that was identified for the deposition of PA6. Powder mixing was conducted for 30 minutes using a 3D motion Turbula shaker mixer (Willy A. Bachofen AG, Switzerland), which incorporates rotation, translation and inversion interactions to ensure homogeneous mixing of powders. This method is effective even for powders with different specific weights and particle sizes. The feed rate was maintained at 4 g/min for spraying of the PA6-30 vol.% Cu powder, while for composite powders with 50 and 75 vol.% Cu, the feed rate was adjusted to 8 and 11 g/min, respectively, aiming to obtain a coating thickness ranging from 500 to 1 mm. Because of the low glass transition temperature and melting point of PA6, the identified cold spray conditions were relatively mild and suboptimal for the deposition of copper. For pure copper deposition, higher cold spray gas temperatures and pressures are typically used to obtain particle impact velocities exceeding the critical velocity, which is the minimum velocity required for successful deposition of the material. With the selected conditions for deposition of the composite coatings, although copper deformation and deposition could be restricted, it was however expected that the substrate surface erosion and damage by the impact of copper particles would be effectively minimized. Under these conditions, it was hypothesized that the polymer matrix within the coatings would provide most of the adhesion strength to the polymeric substrate, while it would act as a binder incorporating the Cu particles and allowing Cu-rich coating buildup. Composite coatings were sprayed

Table 1 List of the cold spray parameters used for the deposition of PA6 powder

Short nozzle	
T_g, °C	260
P_g, MPa	0.41, 0.55, 0.62, 0.76, 0.89
TS, mm/s	10, 20
#passes	1, 2
Long nozzle	
T_g, °C	260
P_g, MPa	0.41, 0.62, 0.82, 1.17, 1.37
TS, mm/s	10
#passes	1

on round pucks (Goodfellow, USA) of 25.4 mm diameter and 6.4 mm thickness. Deposition efficiency was calculated from the ratio of the mass gain of the substrate to the mass of the feedstock powder that was projected on the substrate surface.

Inflight Particles Simulation

CSAM Digital Solutions software (NRC, Canada) was used to simulate the PA6 inflight particle velocity and temperature from the injection to the impact points for each nozzle in addition to the average particle velocity and temperature at impact for the identified optimum spray conditions of PA6. The effect of the substrate on the flow field is fully considered. The 2D axisymmetric subsonic-supersonic compressible flow fields along the nozzle until the substrate were simulated using the open-source SU2 software, which is a widely used implicit finite-volume computational fluid dynamics application. The Menter shear stress transport (SST) $k-\omega$ model is used to compute the turbulent viscosity of the Reynolds-Averaged Navier–Stokes equations. The equations are solved in steady-state using an adaptive time-stepping approach until the relative dimensionless density residual fell below 10^{-11}. The height of the computational domain is set to be 10 times the exit diameter of the nozzle to ensure that there is no interaction between the outer boundary conditions (at ambient pressure and temperature) and the nozzle exit flow. A total-pressure and total-temperature inlet condition was imposed at the entrance of the nozzle, and a symmetric boundary condition is considered along the axis of the nozzle. Sufficient wall resolution (i.e., $y^+ < 1$) was maintained over the nozzle inner and outer walls as well as on the substrate. Depending on the test case, the number of elements in the mesh ranges from about 100,000-20,000

The CFD module of CSAM Digital Solutions was then used to predict the particle velocity and temperature with the flow field solution using a one-way coupled particle tracking approach. This approach assumes that the mean gas flow is not affected by the presence of the particles. Given the small volume fraction of the particles here compared to the volumetric gas flow ($\sim 0.002\%$), such assumption is valid. Newton's second law is integrated for each particle using a fourth order Runge–Kutta scheme. The drag force, the unresolved pressure gradient and the unresolved viscous stress are considered in the force balance. For more details about the inflight particle simulations, please refer to our earlier work (Ref 30). PA6 PSD measured with particle sizing analyzer, melting temperature of 219.5 °C measured with DSC, density of 1.13 g/cm^3 provided by the powder supplier, and specific heat of 1700 J/kg K provided by the powder supplier were used as input parameters for the simulations.

Post-spray Coating Processing

Two post-spray processes of furnace heating and hot pressing were used to improve the cohesion as well as adhesion strength of selected coatings. For both processes, the heating temperature was selected below the melting point of the polymer determined by DSC. Furnace heating tests were performed at 215 °C for 20 min in air, followed by furnace cooling.

Hot press trials were performed using a heated two plates Carver press at a pressure of 400 lbs (508 psi for 25.4 mm dia. samples) and a temperature of 215 °C as shown in Fig. 3. The hot press trials were conducted in three steps: first, the two plates were lowered until they contact the surface of the sample to raise the surface temperature to the hot press temperature of 215 °C without applying any pressure. Once the temperature of the sample surface reached 215 °C, 400 lbs pressure was then applied for 2 min. Finally, the samples were kept on the bench for cooling. The selected temperature, pressure and time were the maximum values permissible without causing the sample to melt or become flattened.

Coating Characterization

Coating quality (uniformity and smoothness) was evaluated from its top surface appearance. Cross-sections of the as-sprayed and processed coatings were analyzed using optical microscopy (BX53M, Olympus-IMS, Japan). The copper content within the coatings was quantified from the optical micrographs using image analysis. Adhesion strength of selected coatings were evaluated according to the ASTM C633 standard test method for adhesion or cohesion strength of thermal spray coatings using an Instron universal testing system (model 5900R, USA). All coatings were ground to a thickness of 500 µm prior to the adhesion tests. LOCTITE 9340 epoxy, treated at 40 °C, was used as the adhesive bonding agent.

Results and Discussion

Window of Deposition for PA6 Powder

The typical DSC heating-cooling curves of PA6 are shown in Fig. 4. Three transitions were observed. The first change of slope occurred around 49.7 °C and is related to T_g of neat PA6 matrix where material starts to be softened. T_g was calculated by the midpoint analysis method, using the midpoint of steps occurred in flow rate curve during the

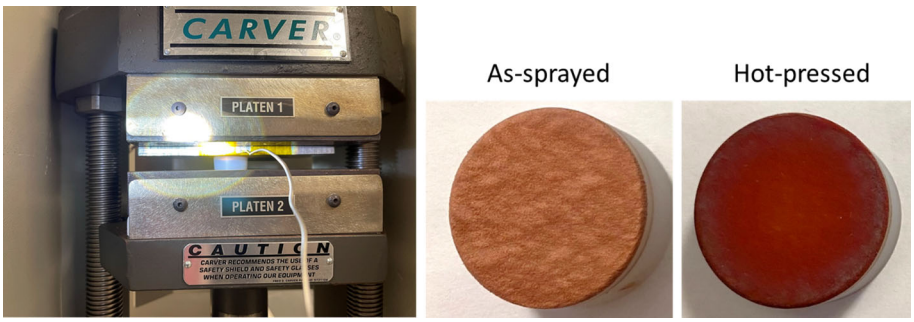

Fig. 3 Temperature monitored Carver hot press process with heated two plates, and PA6-Cu coating as-sprayed and after hot pressing

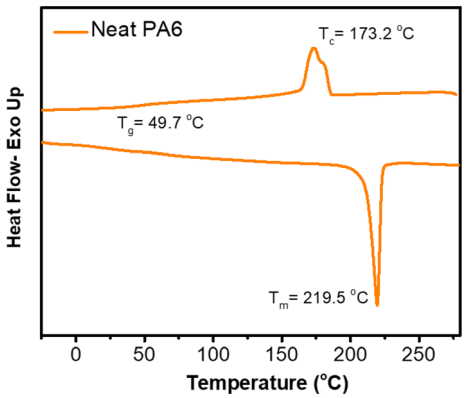

Fig. 4 DSC thermograph of PA6 neat matrix performed at 10 °C/min heating rate under nitrogen atmosphere

cooling cycle. A single melting temperature (T_m) was observed in the heating ramp and represented by endothermal peak at 219.5 °C where all crystalline structure melted. T_m was extracted from the first heating cycle, considering that the material was used in as-received condition, and without prior thermal treatment before the spraying process. Crystallization temperature (T_c) is mainly characterized by exothermal peak, which was observed in the cooling cycle at 173.2 °C.

Considering the downstream powder injection into the diverging section of the nozzle, and therefore short residence time of the powder within the gas jet, a higher temperature than the melting point of the PA6 powder at 260 °C was selected for the gas temperature. This was the maximum temperature that could be used at the lowest selected gas pressure of 0.41 MPa without starting to buildup the powder within the nozzle. At the gas pressure of 0.41 MPa, only a non-continuous thin coating with loosely bonded particles was formed, as shown in Fig. 5(a). By increasing the gas pressure up to 0.76 MPa the coating thickness and deposition uniformity improved progressively as it can be observed in Fig. 5(b), (c) and (d). However, a further increase of the gas pressure to 0.89 MPa was detrimental to the coating quality and partial delamination of the coating occurred (Fig. 5e). Delamination likely resulted from increased thickness, inducing enhanced residual stresses within the coating.

At the gas pressure of 0.76 MPa, increasing the traverse speed from 10 to 20 mm/s had also an adverse effect on coating quality as shown in Fig. 6. The main effect of the traverse speed is on the surface temperature: a higher traverse speed results in a lower surface temperature due to the shorter residence time of the gas jet on the surface, which had a negative effect on coating adhesion to the surface, thus cracking and partial delamination occurred. Although the same total amount of powder was projected on the substrate surface at the two conditions, the deposited coating thickness was lower at the higher traverse speed (1175 µm for 1 pass at 10 mm/s vs. 660 µm for 2 passes at 20 mm/s at the highest point of the coating), indicating an almost double deposition efficiency at the lower gun traverse speed.

With the long nozzle, nozzle clogging occurred at 0.41 MPa of gas pressure. A further increase of the gas pressure up to 0.82 MPa did not lead to particle deposition on the substrate. At 0.82 MPa, only few particles were deposited, and no continuous coating was formed (Fig. 7a). Coating deposition improved significantly at the higher gas pressure of 1.17 MPa, where a uniform coating was formed (Fig. 7b). A further increase of the gas pressure to 1.37 MPa deteriorated the coating quality (Fig. 7c) and craters were formed on the top surface.

These results signify a very narrow window of deposition for the PA6 powder, as a small variation in spray parameters had a significant effect on the coating deposition and quality. A narrow cold spray deposition window is also reported in the literature for a variety of polymeric powders (Ref 31, 32). Khalkhali et al. (Ref 32) associated the narrow deposition window of polyamide to an upper velocity limit, even though a high kinetic energy is needed for inducing plastic deformation and raising the polymer's temperature above its glass transition temperature. In view of these results, the optimum spray conditions for the deposition of PA6 powder at the gas temperature of 260 °C and standoff distance of 10 mm were identified as the gun traverse speed of 10 mm/s, and gas pressures of 0.76 and 1.17 MPa for the short and long nozzles, respectively.

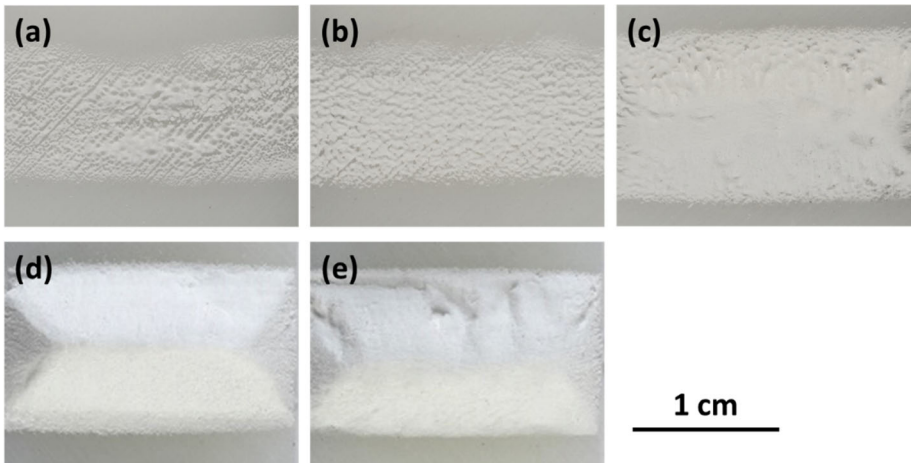

Fig. 5 Top surface photos of PA6 coatings deposited with the short nozzle at the gas temperature of 260 °C and the traverse speed of 10 mm/s after 1 pass and at gas pressures of (a) 0.41 MPa, (b) 0.55 MPa, (c) 0.62 MPa, (d) 0.76 MPa and (e) 0.89 MPa

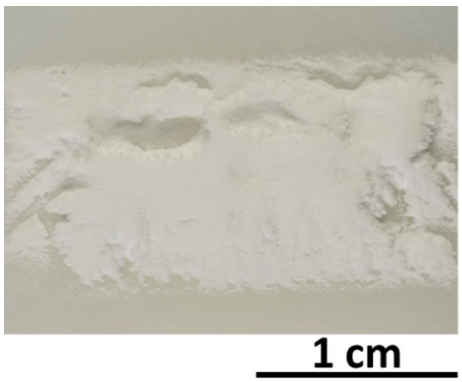

Fig. 6 Top surface of PA6 coating deposited at 260 °C gas temperature, 0.76 MPa gas pressure, 10 mm standoff distance, 20 mm/s traverse speed and 2 passes

Inflight velocity and temperature of 20 µm particles (PA6 d_{50}) along the center axis of the nozzle from the injection point to impact were simulated for the two identified optimum conditions with the short and long nozzles, as well as for the condition with the long nozzle at the gas pressure of 0.41 MPa, where clogging occurred. The simulation results in Fig. 8 show that at 0.41 MPa, the particle velocity significantly dropped about 300 m/s within the long nozzle to the impact point. This drop of particle velocity is due the relatively early appearance of the shock wave within the long nozzle as shown in the Mach number field in Fig. 9. In fact, shock waves were observed inside both long and short nozzles in all three simulated conditions. After the shock waves, the flow velocity under subsonic condition will reduce instead in the diverging section (i.e., act as a diffuser). Therefore, a shock wave occurred further upstream will result in a larger reduction of the flow velocity; hence, leading to a larger decrease in particle velocity. This increases the residence time of the particles within the gas jet. As a result, particle temperature increased above PA6 glass transition temperature, causing particle transition into a rubbery state, and thus material deposition within the nozzle. For the two optimum spray conditions, simulation shows higher particle velocity at impact for the long nozzle. As it can be seen from the Mach number field in Fig. 9, the gas flow expanded supersonically in a longer diverging section of this nozzle at 1.17 MPa; hence the flow was accelerated further. In both nozzles, particle was cooled down from the 40 °C powder pre-heating temperature at the injection point up to the internal shock wave. Bian et al. (Ref 33) made use of such phenomenon of the de Laval nozzle, and proposed a novel liquefaction device for natural gas; in particular, they employed the de Laval nozzle to decrease the gas temperature from 250 K down to the range of 150 K. As observed by Bian et al., the static temperature increases as the flow passes the shock wave (Ref 33). Because of this, the longer supersonic expansion length of the long nozzle also results in a larger temperature drop. Bernard et al. (Ref 34) observed a similar effect for polymer particles inside the nozzle for low inlet gas temperatures. With both nozzles, the particle temperature remained well-below the glass transition temperature of PA6, preventing material buildup and nozzle clogging at the optimum conditions. Taking in to account the whole particle distribution, the average particle velocity and temperature at impact were simulated to be 618 m/s and 15 °C for the short nozzle and 668 m/s and 5 °C for the long nozzle at the identified optimum spray conditions. Considering the low particle temperatures at impact, it is hypothesized that with both nozzles, the hot gas flow (Fig. 9b) increased the surface temperature above the glass transition temperature of PA6, which led to softening of the amorphous fraction of polymer chains in both substrate and deposited particles, thereby facilitating deposition of the impacting particles on the surface at high velocities. For these coatings, influence of the low-temperature particles on surface temperature is expected to be negligible, as it has been shown that the heat

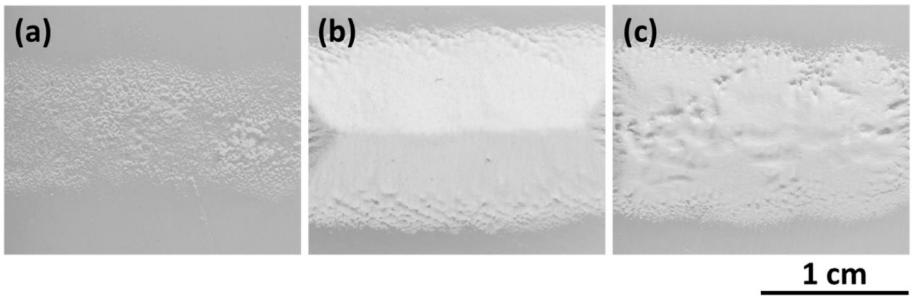

Fig. 7 Top surface photos of PA6 coatings deposited with the long nozzle at gas temperature of 260 °C and traverse speed of 10 mm/s after 1 pass and at gas pressures of (a) 0.82 MPa, (b) 1.17 MPa, (c) 1.37 MPa

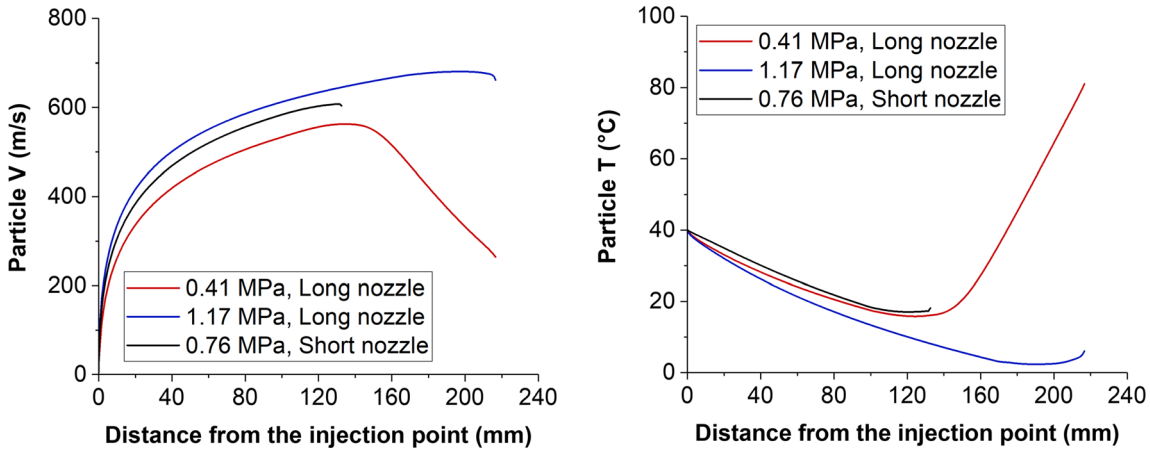

Fig. 8 Simulated inflight particle (20 μm) velocity and temperature from injection point to impact along the centerline of the short and long nozzles for selected spray conditions

exchange between the impacting particles and the surface is minimal compared to the gas jet and the surface (Ref 35). Localized heating generated by high velocity impact of the particles on the surface may have also contributed to their deposition. The higher deposition efficiency of 23% with the long nozzle, compared to 12% with the short nozzle, shows that increase of the particle velocity had a more significant influence on particle deposition than the temperature.

Deposition of Composite Coatings

The identified optimum cold spray conditions for the deposition of the PA6 powder with each of the nozzle geometries were employed to deposit the three composite powder mixtures with different copper contents of 30, 50 and 75 vol.%. Top surface photos and cross-sectional images of the produced coatings are shown in Figs. 10 and 11. In the cross-sectional images, the copper particles appear as the bright phase, the PA6 matrix as the gray phase and the pullouts during the metallographic preparation and porosities as black areas.

From the top surface photos, it is clear that increasing the copper content in the mixture as well as using the long nozzle were advantageous to improve coatings uniformity. The top surface of the coating that was sprayed with the PA6-30 vol.% Cu powder with the short nozzle (Fig. 10a) appears to have polymer-rich and copper-rich zones demonstrated by formation of a feathery patterned coating. In the cross-sectional micrograph of this coating in Fig. 11(a), the two copper and polymer rich zones are also discernible. It is hypothesized that the large difference between PA6 and Cu particle temperature and velocity due to the differences in material properties, such as density and specific heat, caused insufficient bonding between the deposited particles and resulted in formation of such surface pattern. The cross-sectional micrograph also shows that the copper particles did not plastically deform and they retained their spherical morphology. Large number of pullouts indicates low adhesion between the deposited Cu and PA6 particles. The image analysis results showed a copper content of 11.3% within the coating. However, considering the pullouts, this value is largely underestimated and it is not representative of the actual retained copper content. A deposition efficiency of 52% was obtained for this coating, well-above the deposition efficiency of PA6 powder without Cu addition. Increase of deposition efficiency by adding a secondary component is reported in the literature and is related to the tamping effect of the secondary component particles with a higher

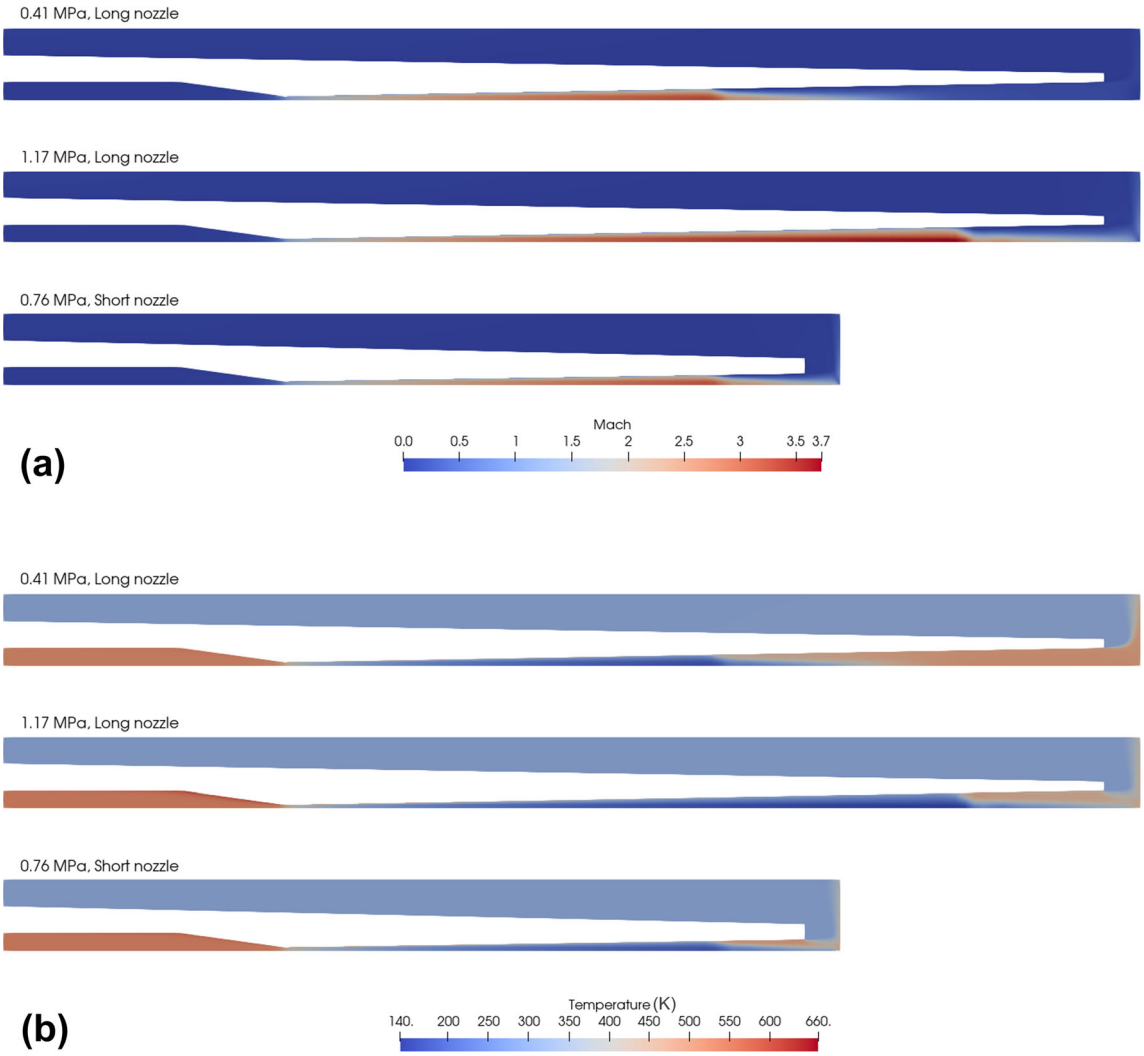

Fig. 9 (a) Mach number and (b) temperature along the domain for three selected conditions

hardness (Ref 24). With the long nozzle, the top surface of the coating with the same copper content in the mixture appears to be more uniform (Fig. 10b), which could be explained by the higher impact velocity of the particles when using this nozzle. The lower number of pullouts (Fig. 11b) and a higher copper content of 19.3% obtained for this coating indicate a better bonding between the Cu and PA6 deposited particles. However, the deposition efficiency was at 34%, lower than that of the short nozzle, signifying a larger number of rebound particles and/or higher surface erosion of the polymer by the copper particles impacting the surface at higher velocities, yielding a more uniform surface profile. The interface of both coatings with the substrate appears to be undamaged by the impinging particles as no Cu particle penetration into the substrate could be seen, contrary to what is typically observed when spraying metallic particles directly on to a polymer substrate (Ref 28, 36).

Coating deposited using the PA6-50 vol.% Cu mixture and the short nozzle is shown in Figs. 10(c) and 11(c). The surface morphology appears to be non-uniform, however due to the presence of more copper, formation of segregated nylon and Cu-rich zones were not evident on the top surface. Copper dispersion within the microstructure also appears to be more uniform than the coating with 30% Cu. Again, a more uniform surface morphology was obtained for the coating deposited with the long nozzle as shown in Fig. 10(d). Addition of more copper to the powder mixture resulted in higher copper contents of 26 and 28% for the coatings deposited with the short and long nozzles, respectively. As the copper content in the feedstock is increased, the deposition efficiency decreased. A deposition efficiency of 25% was obtained for the coating made

with the long nozzle compared to 40% for the one made with the short nozzle. A lower number of pullouts in both coatings compared to those made with the PA6-30 vol.% Cu mixture could be associated with improved coating cohesion related to surface peening by a larger number of impacting Cu particles.

Figure 10(e) and (f) show that a uniform surface morphology was obtained for the coatings that were sprayed with the PA6-75 vol.% Cu mixture with both nozzles. The reduced surface texture of the composite coatings by increasing the harder phase content in the powder blend has been related to the tamping effect induced by the impact of the hard phase on the previously deposited layers (Ref 24, 37, 38). The copper content was further increased to 30% for the coating sprayed with the short nozzle and 41% for the coating sprayed with the long nozzle, as shown in Fig. 11(e) and (f). Within the microstructure of the coating deposited using the long nozzle (Figs. 11(f) and 12), deformation of Cu particles is noticeable. This could be explained by a higher probability of the high velocity Cu particles impacting onto the deposited Cu particles as the Cu content is higher in the starting powder mixture. Although the velocity of the metallic particles may not be high enough for their effective bonding to the deposited metallic particles, the high velocity impact induces peening effect, coating compaction and deformation of the deposited particles. A similar effect was observed by Qiu et al. (Ref 37) when spraying powder blends of Al_2O_3 and aluminum. Although increase of Cu content in the powder mixture is favorable for improving coating cohesion as illustrated by a lower number of pullouts, it is detrimental to the coating deposition efficiency which was further reduced to 11% for both coatings sprayed with the short and long nozzles. The employed suboptimal spray conditions lead to a more excessive Cu particle rebounding and surface erosion resulting in a reduced deposition efficiency.

Independent of the copper percentage in the powder mixtures, the higher copper content retained within the coating microstructures during metallographic preparation and the lower number pullouts are indications of a better coating cohesion when the long nozzle was used. For these coatings, mechanical hammering of the deposited layers by the impacting Cu particles is responsible for reinforcement of the polymer matrix by formation of stronger bonds among the deposited particles, more coating compaction and thus improved cohesion.

In light of these results, spraying composite powders of high copper content while employing the long nozzle is advantageous for retaining a high copper concentration within the microstructure. This was demonstrated by a significant increase of the copper content in the coating from 11.3 to 41%, while the porosity and pullouts reduced from 27 to 16% when transitioning from spraying PA6-30 vol.% Cu with the short nozzle to PA6-75 vol.% Cu with the long nozzle.

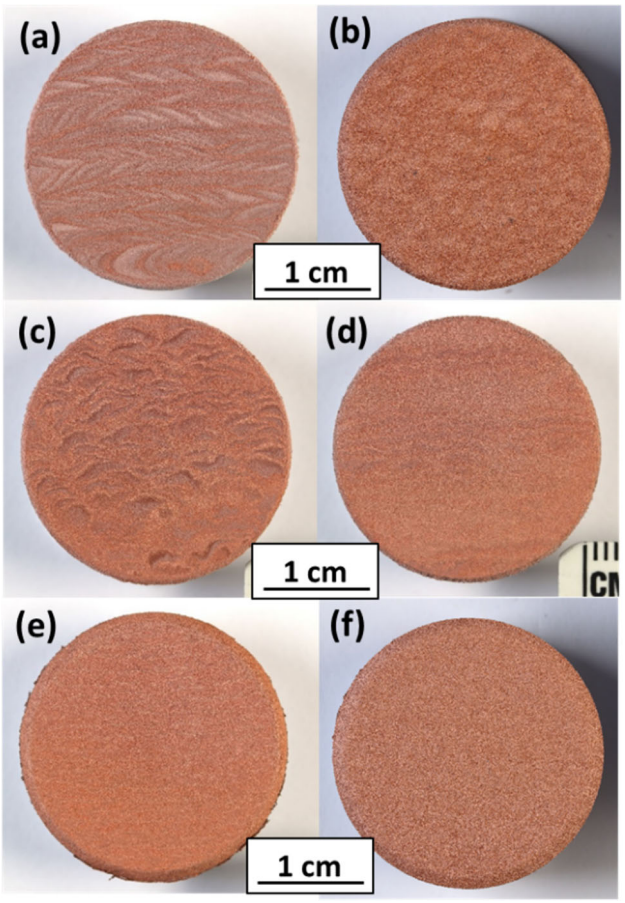

Fig. 10 Top surface photos of the PA6-Cu composite coatings deposited using powder mixtures with the Cu content of (a, b) 30 vol.%, (c, d) 50 vol.% and (e, f) 75%; and made with the (a, c, e) short nozzle and (b, d, f) long nozzle

Post Spray Coating Processing

To improve bonding between the deposited Cu and PA6 particles, furnace heating and hot pressing of selected deposits were examined. The hot press pressure was selected to slightly compact the coating without causing damage to the coating or deforming the substrate. Figures 13 and 14 show the cross-sectional micrographs of selected post-processed coatings deposited with powder mixtures containing 50 and 75 vol.% of Cu, respectively. Copper content and adhesion/cohesion strength of these coatings compared to their as-sprayed counterparts are shown in Table 2. The results show that a higher copper content was retained within the microstructure after hot pressing while there was a slight to no change after furnace heating. This implies that coating compaction by pressing is required besides softening of the polymer matrix to

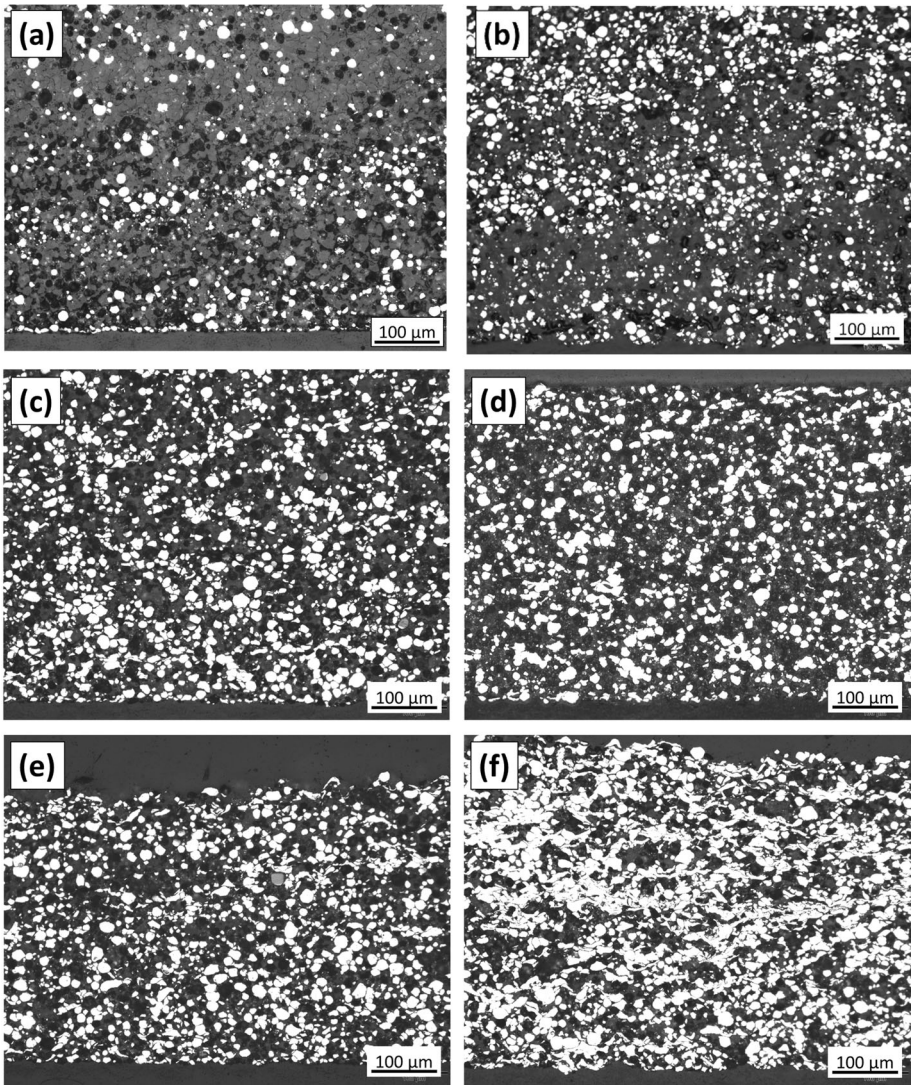

Fig. 11 Cross-sectional micrographs of the PA6-Cu composite coatings with Cu content of (a, b) 30 vol.%, (c, d) 50 vol.% and (e, f) 75 vol.%; and made with the (a, c, e) short nozzle and (b, d, f) long nozzle

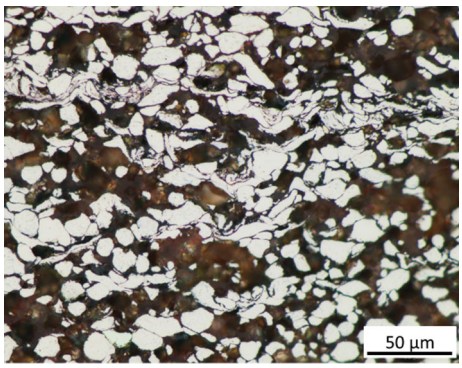

Fig. 12 Copper particle deformation in the composite coating made with the PA6-75 vol.% Cu powder cold sprayed using the long nozzle

provide a stronger grip between the copper particles and the polymer matrix, hence improving coating cohesion and reducing the number of pullouts.

All as-sprayed and post-processed samples demonstrated cohesive failure within the coatings. The results in Table 2 show that the cohesion strength for all the as-sprayed coatings was less than 1.6 MPa, except for the coating deposited using the long nozzle with 75% Cu content; for which, the cohesion strength was $\sim$ 5 MPa. It seems that impact of a larger number of particles at higher velocities resulted in a superior coating cohesion. Both post processing methods yielded improved coatings cohesion strength. It is expected that softening of the polymer matrix at temperatures slightly below its melting point enhanced the bonding between the deposited particles, and improved the cohesion strength. Hot-pressed coatings had a slightly better cohesion than the heat-treated samples demonstrating the positive effect of coating compaction to enhance particle bonding.

To better evaluate the amount of the retained copper in the coatings without having the effect of particles pullout

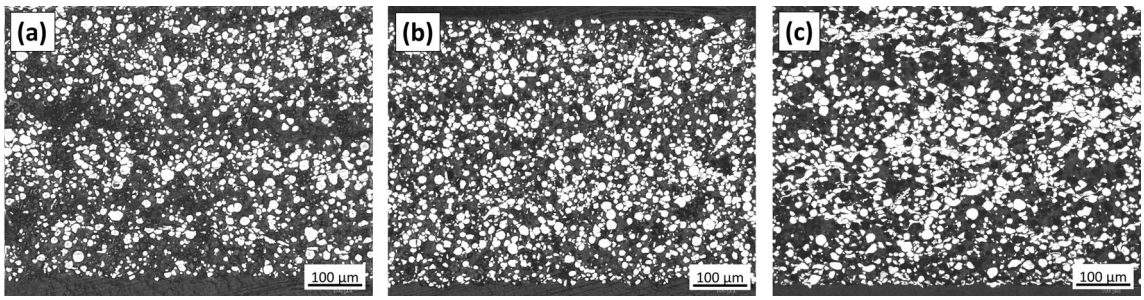

Fig. 13 Cross-sectional micrographs of composite coatings sprayed with PA6- 50 vol.% Cu powder after post processing (a) short nozzle, furnace heated (b) short nozzle, hot pressed and (c) long nozzle, hot pressed

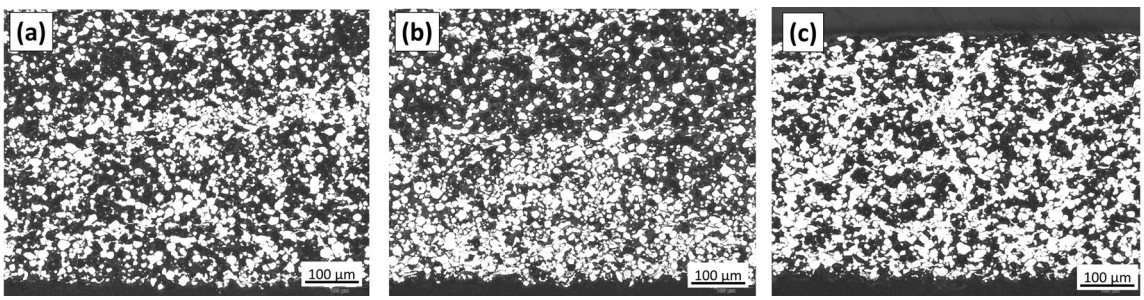

Fig. 14 Cross-sectional micrographs of composite coatings sprayed with PA6- 75 vol.% Cu powder after post processing (a) short nozzle, furnace heated (b) short nozzle, hot pressed and (c) long nozzle, hot pressed

Table 2 copper content and adhesion/cohesion strength of as-sprayed, heat-treated and hot pressed PA6-Cu coatings cold sprayed with the short and the long nozzles

Powder mixture composition	Coating condition	Cu content in coating*, %		Adhesion/cohesion strength, MPa	
		Short nozzle	Long nozzle	Short nozzle	Long nozzle
PA6-50 vol.% Cu	As-sprayed	26	28	1.1 ± 0.2	1.6 ± 0.2
	Heat-treated	28	…	5.3 ± 0.8	…
	Hot-pressed	32	36	5.7 ± 0.9	5.5 ± 0.3
PA6-75 vol.% Cu	As-sprayed	30	41	1.3 ± 0.2	5.1 ± 0.4
	Heat-treated	30	…	5.3 ± 0.7	…
	Hot-pressed	40	49	6.2 ± 0.9	6.0 ± 1.2

*The reported values are based on image analysis (area%) form the coating microstructures, and are under-estimated from the actual copper content due to the pullouts

by polishing, images were taken from the hot-pressed coating microstructures after the cutting step and prior to polishing, as shown in Fig. 15. The results show that the same copper content of 57% was obtained for the coatings sprayed with the PA6-50 vol.% Cu mixture and the two nozzles. For the coatings that were sprayed with the PA6-75 vol.% Cu mixture, a copper content of 76% was obtained with the long nozzle whereas it was lower at 67% with the short nozzle. The results show that when the copper percentage in the starting mixtures exceeds a certain threshold, using the long nozzle that yields a higher particle impact velocity is beneficial for increasing the deposition of copper in composite coatings.

Conclusions

This study explored the feasibility of combining cold spraying and post spray coating processing to obtain coatings of high copper content with improved adhesion/cohesion strength. For cold spray deposition, an approach of spraying PA6-Cu powder mixtures was used for the deposition of the composite coatings. This approach

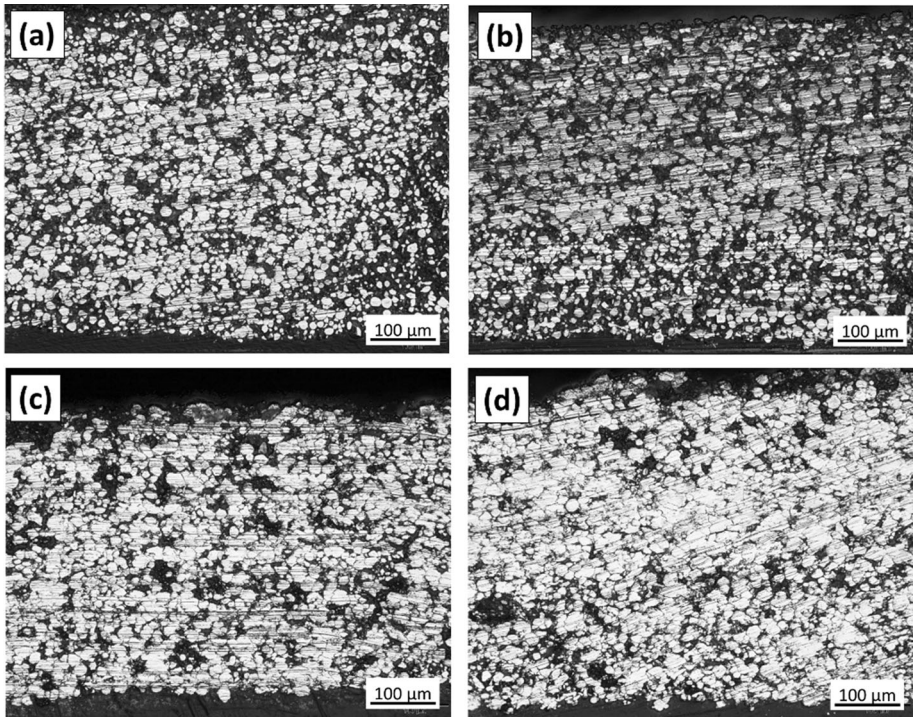

Fig. 15 Cross-sectional micrographs of hot-pressed composite coatings after cutting and prior to polishing, presenting more accurately the copper content within the coatings by minimizing the pullouts (a) PA6- 50 vol.% Cu, short nozzle, (b) PA6- 50 vol.% Cu, long nozzle, (c) PA6- 75 vol.% Cu, short nozzle and (d) PA6- 75 vol.% Cu, long nozzle

relies on the formation of a soft polymer matrix acting as a binder to incorporate a network of hard Cu particles. Composite coatings of high thickness were successfully deposited on PA6 substrates using a low-pressure cold spray system. The spray parameters were first developed for the deposition of the PA6 powder using two nozzle geometries with different length of the diverging sections. The respective optimal conditions were then used to deposit the composite coatings with 30, 50 and 75 vol.% of Cu. Surface uniformity and cross-sectional homogeneity of the coatings were improved by increasing the Cu content in the mixture and using the long nozzle. Higher copper content of 75 vol.% promoted the tamping effect induced by the impact of the hard Cu particles on the previously deposited layer. The tamping effect besides higher velocity of the particles with the long nozzle, resulted in increased number of retained Cu particles in the coating, more deformation of the deposited Cu particles and higher cohesion strength of the coating. To further improve the cohesion strength, furnace heating and hot pressing of selected deposits were examined. The results revealed a minimum of fourfold increase in the cohesion strength of the coatings that were sprayed with the short nozzle. The highest cohesion strength of $\sim$ 6 MPa and copper content of 67-75% was obtained for the coatings that were sprayed with PA6-75 vol.% Cu mixture after hot-pressing. The obtained results demonstrate the effectiveness of the combined cold spray and post-processing approach in achieving substantial Cu deposition on the polymer surface. While this study primarily focused on improving deposition and cohesion of the PA6-Cu composite coatings, future work will involve performing conductivity assessments to evaluate the electrical properties of the coatings, which will provide valuable insights into their suitability for various applications.

Funding Open Access funding provided by National Research Council Canada.

References

1. M. Monteforte, Polymer-Matrix Composites, Technology Map-Business Opportunities in Technology Commercialization, Strategic Business Insights, Explorer, 2017.
2. M. Adamu, M.R. Rahman, R. Baini and M.K.B. Bakri, Applications of Sustainable Polymer Composites in Automobile and

Aerospace Industry, *Adv. Sustain. Polym. Compos.*, 2021, p 185-207.
3. M. Pervaiz, S. Panthapulakkal, M. Sain and J. Tjong, Emerging Trends in Automotive Lightweighting Through Novel Composite Materials, *Mater. Sci. Appl.*, 2016, **7**(1), p 26-38.
4. R. Lupoi, C. Stenson, K.A. McDonnell, D.P. Dowling and E. Ahearne, Antifouling Coatings Made with Cold Spray onto Polymers: Process Characterization, *CIRP Ann.*, 2016, **65**(1), p 545-548.
5. R. DellaGatta, A.S. Perna, A. Viscusi, G. Pasquino and A. Astarita, Cold Spray Deposition of Metallic Coatings on Polymers: A Review, *J. Mater. Sci.*, 2021, **57**, p 27-57.
6. Y. Yao, S. Jin, H. Zou, L. Li, X. Ma, G. Lv, F. Gao, X. Lv and Q. Shu, Polymer-Based Lightweight Materials for Electromagnetic Interference Shielding: A Review, *J. Mater. Sci.*, 2021, **56**, p 6549-6580.
7. R. Gonzalez, H. Ashrafizadeh, A. Lopera, P. Mertiny and A. McDonald, A Review of Thermal Spray Metallization of Polymer-Based Structures, *J. Therm. Spray Technol.*, 2016, **25**, p 897-919.
8. H. Parmar, F. Tucci, P. Carlone and T.S. Sudarshan, Metallisation of Polymers and Polymer Matrix Composites by Cold Spray: State of the Art and Research Perspectives, *Int. Mater. Rev.*, 2021, **67**(4), p 385-409.
9. R. Melentiev, N. Yu and G. Lubineau, Polymer Metallization via Cold Spray Additive Manufacturing: A Review of Process Control, Coating Qualities, and Prospective Applications, *Addit. Manuf.*, 2021, **48**(1), p 102459.
10. A. Astarita, L. Boccarusso, L. Carrino, M. Durante, A.S. Perna, A. Viscusi, Cold Spray Deposition on Polymeric and Composite Substrates, *Cold spray in the realm of additive manufacturing*, 2020, p 87-128.
11. A. Papyrin, V. Kosarev, K.V. Klinkov and V.M. Fomin, *Cold Spray Technology*, Elsevier Ltd., London, 2006.
12. V.K. Champagne, *The Cold Spray Deposition Process: Fundamentals and Applications*, Woodhead Publishing Ltd., Cambridge, 2007.
13. J. Villafuerte, *Modern Cold Spray: Materials, Process, and Applications*, Springer, Berlin, 2015.
14. D. Zhang, P. Shipway and D. McCartney, Cold Gas Dynamic Spraying of Aluminum: The Role of Substrate Characteristics in Deposit Formation, *J. Therm. Spray Technol.*, 2005, **14**, p 109-116.
15. H. Che, P. Vo and S. Yue, Metallization of Carbon Fiber Reinforced Polymers by Cold Spray, *Surf. Coat. Technol.*, 2017, **313**, p 236-247.
16. C. Chen, X. Xie, Y. Xie, X. Yan, C. Huang, S. Deng, Z. Ren and H. Liao, Metallization of Polyether Ether Ketone (PEEK) by Copper Coating via Cold Spray, *Surf. Coat. Technol.*, 2018, **342**, p 209-219.
17. H. Che, A.C. Liberati, X. Chu, M. Chen, A. Nobari, P. Vo and S. Yue, Metallization of Polymers by Cold Spraying with Low Melting Point Powders, *Surf. Coat. Technol.*, 2021, **418**, 127229.
18. A. Ganesan, M. Yamada and M. Fukumoto, Cold Spray Coating Deposition Mechanism on the Thermoplastic and Thermosetting Polymer Substrates, *J. Therm. Spray Technol.*, 2013, **22**(8), p 1275-1282.
19. P. Fallah, R. Chakrabarty, J. Song, A. McDonald and S. Yue, Effect of Metallic Interlayer Hardness on Deposition Characteristics of Cold-Sprayed Copper Particles on Carbon Fiber-Reinforced Polymers, *J. Therm. Spray Technol.*, 2022, **21**, p 559-573.
20. F. Robitaille, M. Yandouzi, S. Hind and B. Jodoin, Metallic Coating of Aerospace Carbon/Epoxy Composites by the Pulsed Gas Dynamic Spraying Process, *Surf. Coat. Technol.*, 2009, **203**(19), p 2954-2960.
21. A. Ganesan, J. Affi, M. Yamada and M. Fukumoto, Bonding Behavior Studies of Cold Sprayed Copper Coating on the PVC Polymer Substrate, *Surf. Coat. Technol.*, 2012, **207**, p 262-269.
22. A. Małachowska, M. Winnicki, Ł Konat, T. Piwowarczyk, L. Pawłowski, A. Ambroziak and M. Stachowicz, Possibility of Spraying of Copper Coatings on Polyamide 6 With Low Pressure Cold Spray Method, *Surf. Coat. Technol.*, 2017, **318**, p 82-89.
23. X.L. Zhou, A.F. Chen, J.C. Liu, X.K. Wu and J.S. Zhang, Preparation of Metallic Coatings on Polymer Matrix Composites by Cold Spray, *Surf. Coat. Technol.*, 2011, **206**(1), p 132-136.
24. H. Che, X. Chu, P. Vo and S. Yue, Cold Spray of Mixed Metal Powders on Carbon Fiber Reinforced Polymers, *Surf. Coat. Technol.*, 2017, **329**, p 232-243.
25. H. Che, A. Liberati, P. Vo, S. Yue, Cold Spray of Mixed Sn-Zn and Sn-Al Powders on Carbon Fiber Reinforced Polymers, *Mater. Sci. Forum*, 2018, p 1892-1897.
26. A. Liberati, H. Che, M. Aghasibeig, K.R. Yu, P. Vo and S. Yue, On the Importance of Secondary Component Properties for Cold Spray Metallization of Carbon Fiber Reinforced Polymers, *J. Therm. Spray Technol.*, 2022, **21**, p 159-175.
27. A.C. Liberati, H. Che, P. Vo and S. Yue, Influence of Secondary Component Hardness When Cold Spraying Mixed Metal Powders on Carbon Fiber Reinforced Polymers, *J. Therm. Spray Technol.*, 2021, **30**, p 1239-1253.
28. V. Bortolussi, B. Figliuzzi, F. Willot, M. Faessel and M. Jeandin, Electrical Conductivity of Metal-Polymer Cold Spray Composite Coatings onto Carbon Fiber-Reinforced Polymer, *J. Therm. Spray Technol.*, 2020, **29**(4), p 642-656.
29. F. Delloro, A. Chebbi, H. Perrin, G. Ezo'o, A. Bastien, J. Ascani, A. Tazibt, Cold Spray of Metallic Coatings on Polymer Based Composites for the Lightning Strike Protection of Airplane Structures, *Proc. Int. Therm. Spray Conf.*, 2021, p 87-95.
30. D. Poirier, J.-G. Legoux, P. Vo, B. Blais, J.D. Giallonardo and P.G. Keech, Powder Development and Qualification for High-Performance Cold Spray Copper Coatings on Steel Substrates, *J. Therm. Spray Technol.*, 2019, **28**, p 444-459.
31. N.K. Singh, K.Z. Uddin, J. Muthulingam, R. Jha and B. Koohbor, Analyzing the Effects of Particle Diameter in Cold Spraying of Thermoplastic Polymers, *J. Therm. Spray Technol.*, 2021, **30**(5), p 1225-1238.
32. Z. Khalkhali and J.P. Rothstein, Characterization of the Cold Spray Deposition of a Wide Variety of Polymeric Powders, *Surf. Coat. Technol.*, 2020, **383**, 125251.
33. J. Bian, X. Cao, W. Yang, M.A. Edem, P. Yin and W. Jiang, Supersonic Liquefaction Properties of Natural Gas in the Laval Nozzle, *Energy*, 2018, **159**, p 706-715.
34. C.A. Bernard, H. Takana, G. Diguet, K. Ravi, O. Lame, K. Ogawa and J.-Y. Cavaillé, Thermal Gradient of In-Flight Polymer Particles During Cold Spraying, *J. Mater. Process. Technol.*, 2020, **286**, 116805.
35. V. Kosarev, S. Klinkov, A. Alkhimov and A. Papyrin, On Some Aspects of Gas Dynamics of the Cold Spray Process, *J. Therm. Spray Technol.*, 2003, **12**, p 265-281.
36. A. Viscusi, M. Durante, A. Astarita, L. Boccarusso, L. Carrino and A.S. Perna, Experimental Evaluation of Metallic Coating on Polymer by Cold Spray, *Procedia Manuf.*, 2020, **47**, p 761-765.
37. X. Qiu, J.Q. Wang, J.R. Tang, L. Gyansah, Z.P. Zhao and T.Y. Xiong, Microstructure, Microhardness and Tribological Behavior of Al2O3 Reinforced A380 Aluminum Alloy Composite Coatings Prepared by Cold Spray Technique, *Surf. Coat. Technol.*, 2018, **350**, p 391-400.
38. K.I. Triantou, D.I. Pantelis, V. Guipont and M. Jeandin, Microstructure and Tribological Behavior of Copper and Composite Copper+Alumina Cold Sprayed Coatings for Various Alumina Contents, *Wear*, 2015, **336**, p 96-107.